

# Fragility analysis of concrete-filled steel tube arch bridge subjected to near-fault ground motion considering the wave passage effect

Zhen Liu\* and Zhe Zhang

School of Civil Engineering, Dalian University of Technology, Dalian, 116024, China

(Received June 19, 2016, Revised November 22, 2016, Accepted December 28, 2016)

**Abstract.** This paper focuses on the impact of the wave passage effect on the long-span bridge. In order to make the wave passage effect more obvious, ground motion samples are selected from the near-fault ground motion of the 1999 Chi-Chi earthquake and an arch bridge with a 280m main span is selected as a bridge sample. The motion ground samples are divided into two groups according to the characteristics of near-fault. A sequence of fragility curves is developed. It is shown that the seismic damage is increased by the wave passage effect and the increase is more obvious in the near-fault ground motion.

**Keywords:** wave passage effect; near-fault ground motion; seismic fragility; concrete-filled steel tube arch bridges

## 1. Introduction

The spatial and temporal features of seismic waves vary during their propagating processes. The spatial variation can be ignored for small-size structures. However, the seismic damage of the large-size structures can be largely underestimated when the spatial variation is ignored (Todorovska and Trifunac 1989). Long span bridges are often used in lifeline projects so that the wave passage effect has been studied by many researchers. For example, a suspension bridge had been analyzed using the random vibration methodology when it was subjected to spatially varying ground motion (Zhang *et al.* 2009). The fragility curves of multi-span bridges were developed considering the influence of the spatial variability of ground motion (Saxena 2000, Deodatis 2000).

The spatial variation of seismic ground motion can be attributed to three sources: the time difference of arrival of ground motion between two locations, referred to as the “wave passage effect”; the change in shape of the waveform because of the reflections and refractions of seismic wave, known as the “incoherence effect”; the change in frequency and amplitude of seismic wave because of the different soil condition at different locations, referred to as the “local site effect” (Sang-Hoon *et al.* 2003). It is proved that the seismic damage of the long span bridge is underestimated if the wave passage effect is ignored (Bi *et al.* 2013). In recent years, the fragility analysis is used to study the wave passage effect (Mehanny *et al.* 2014).

The near-fault ground motions are considered as the most dangerous earthquake, which has been demonstrated by many researchers in major earthquakes (Somerville *et al.* 1997, Akkar 2005). Ground motions can be divided into 2 types by the distance between the point at which they are

recorded and the fault line. The ground motions which are recorded within 15 km to the fault line can be defined as near-fault ground motions. Far-fault ground motions are recorded at a distance more than 15 km (Billah *et al.* 2013). The long-period pulse and permanent ground displacement are contained in near-fault ground motions (Somerville 2002). Because of the long-period pulse, the wave effect can be intensified by the near-fault ground motion. In the 1999 Chi-Chi earthquake, the town of Chi-Chi is situated at two major fault lines and many buildings are close to the major fault lines. Most of the collapses of bridges are happened near the fault lines. (Yao and Chung 2004)

In the study, a three-dimensional (3D) finite element model is built to obtain the seismic response. A set of ground motions from the 1999 Chi-Chi earthquake is selected as the ground motion input. A concrete-filled steel tube (CFST) arch bridge is modeled using finite element analysis (FEA) program. In order to quantify the seismic damage, a strain and energy based damage model is used to evaluate the seismic response. The damage change caused by the wave passage effect is estimated using the seismic fragility analysis.

## 2. Seismic damage

A strain and energy based damage model is used to evaluate the seismic damage of the CFST arch bridge. The damage model is based on the Park-Ang double parameter failure criterion (Young and Alfredo 1985), which can be defined as

$$D = \frac{\delta_M}{\delta_u} + \frac{\beta}{Q_y \delta_u} \int dE \quad (1)$$

where  $D$  is the damage index according to the Park-Ang failure criterion;  $\delta_u$  is the limit deformation of the component;  $\delta_M$  is the maximum deformation in structural

\*Corresponding author  
E-mail: liuzhen1988@mail.dlut.edu.cn

finite element analysis;  $Q_y$  is the yield strength value of the component;  $E$  is the cumulative hysteretic energy of the component;  $\alpha$  is a damage coefficient.

Some changes are made to achieve a good performance in the Par-Ang failure criterion because of the features of the CFST arch bridge (Xie *et al.* 2012). The adjusted damage model can be expressed as

Arch rib

$$I_{ar} = \frac{\lambda_m}{\lambda_u} + \alpha \frac{\int E_h dl}{\int (N_u \varepsilon_u + a M_u \varphi_u) dl} \quad (2)$$

Suspender

$$I_{su} = \frac{\varepsilon_m}{\varepsilon_u} + \alpha \frac{\int E_h dl}{\int N_u \varepsilon_u dl} \quad (3)$$

Beam

$$I_{be} = \frac{\varepsilon_m}{\varepsilon_u} + \alpha \frac{\int E_h dl}{\int M_u \varphi_u dl} \quad (4)$$

where  $I_{ar}$ ,  $I_{su}$ , and  $I_{be}$  are the damage index of one arch rib member, one suspender member and one beam member, respectively;  $\lambda_m$  is the maximum ratio between the bending moment and axial force of the arch rib member under earthquake;  $\lambda_u$  is the limit ratio between the bending moment and axial force of the arch rib member;  $\varepsilon_m$  is maximum strain of the member under earthquake;  $\varepsilon_u$  is the limit strain of the member;  $N_u$  is the limit axial force of the member;  $M_u$  is the limit bending moment of the member;  $\varphi_u$  is the limiting curvature of a member;  $E_h$  is the cumulative hysteretic energy of the member under the earthquake;  $l$  is the length of the member;  $\alpha$  is a coefficient, and  $\alpha=0.139$  as suggested by the paper (Young and Alfredo 1985).

The damage index of the entire bridge is calculated by the damage index of each part of the bridge. The weight of each part damage index on the entire damage index is calculated by the percentage of the cumulative hysteretic energy on the total energy under the earthquake.

According to this rule, the damage index of the whole bridge can be defined as

$$I = I_{ar} W_{ar} + I_{su} W_{su} + I_{be} W_{be} \quad (5)$$

The weight of suspenders damage index on the whole bridge damage index can be defined as

$$W_{su} = E_{su} / (E_{ar} + E_{su} + E_{be}) \quad (6)$$

where  $I_{ar}$ ,  $I_{su}$ ,  $I_{be}$  are the damage indexes of the whole arch rib, suspender and beam, respectively;  $W_{ar}$ ,  $W_{su}$ ,  $W_{be}$  are the weight values of the whole arch rib, suspender and beam, respectively;  $E_{ar}$ ,  $E_{su}$ ,  $E_{be}$  are the cumulative hysteretic energy of arch rib, suspender and beam under the earthquake, respectively.

In accordance with the principle above, the damage index of each part can be calculated by the damage of their members. For example, the damage index of the suspender is defined as follows

Table 1 Damage index range of bridge structure under different damage degrees

Damage level	Damage index range
No damage state	0.00~0.10
Slight damage state	0.10~0.30
Moderate damage state	0.30~0.50
Extensive damage state	0.50~0.70
Collapse damage state	0.70~1.00

$$\begin{cases} I_{su} = \sum (W_j)_{su} (I_j)_{su} \\ (W_j)_{su} = \frac{(E_j)_{su}}{\sum (E_i)_{su}} \end{cases} \quad (7)$$

where  $j$  is the number of each suspender members;  $\sum$  means the summation;

The relationship between the seismic demand and seismic capacity is defined by this damage model. The different degrees of seismic damage can be described by the index damage. According to the paper (Mario *et al.* 2009), the range of each damage level can be defined as Table 1.

### 3. Fragility analysis

The bridge fragility is described as the conditional probability under a given ground motion intensity. A formula can be established using mathematical methods according to the definition. (Karim *et al.* 2009)

$$P_f = P \left[ \frac{S_d}{S_c} \geq 1 \right] \quad (8)$$

where  $P_f$  is the conditional probability;  $S_d$  is the structural seismic demand;  $S_c$  is the structural seismic capacity. Random variables  $S_d$  keep linear relationship with ground motion intensity under the logarithmic coordinates according to the study (Hwang *et al.* 2009). Then the above formula can be expressed as follows

$$P_f = \Phi \left[ \frac{\mu_d / \mu_c}{\sqrt{\beta_d^2 + \beta_c^2}} \right] \quad (9)$$

where  $\mu_d$  and  $\mu_c$  are the means of  $\ln(S_d)$  and  $\ln(S_c)$ ;  $\beta_d$  and  $\beta_c$  are the standard deviations of  $\ln(S_d)$  and  $\ln(S_c)$ . In a previous study (Karim *et al.* 2000), the structural seismic capacity is based on a certain damage level and the structural seismic demand is obtained by finite element calculation.

In this work, the damage index is used to evaluate the seismic damage. Then the ratio of the structural demand and capacity is replaced by the damage index and the formula is expressed as follows

$$P_f = P [I > I_i] = \Phi \left[ \frac{\ln(I/I_i)}{\beta} \right] \quad (10)$$

where  $I_i$  is the damage index of a certain damage level;  $\beta$  is the standard deviation of  $\ln(I)$ .

#### 4. Bridge model

The purpose of this paper is to study to the influence of the wave passage effect on the damage of the bridge. In order to make this effect more obvious, no material or geometric uncertainty is involved. The dimensions of the CFST arch bridge are shown in the Figs. 1 and 2. The analysis is conducted by the ANSYS program and the 3-D FEA model is shown in Fig. 3.

The arch rib and beam are modeled as beam elements (BEAM189). The suspender is modeled as truss elements (LINK10). The bridge deck is modeled as mass elements (MASS21). Stress-strain relationship of steel is simplified into ideal elasto-plastic to simplify the calculation (Eq. (11) and Eq. (12)). Stress-strain relationship of concrete is assumed as the Hognestad model (Hognestad 1951) (Eq. (13) and Eq. (14)). The CFST is different from the steel and concrete in the mechanical properties. According to the study (Wang *et al.* 2009), the stress-strain relationship can be shown as (Eq. (15) and Eq. (16)).

$$\varepsilon \leq \varepsilon_y \quad \sigma = E_y \varepsilon \quad (11)$$

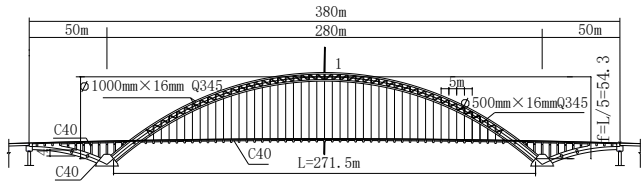


Fig. 1 Elevation of the CFST arch bridge

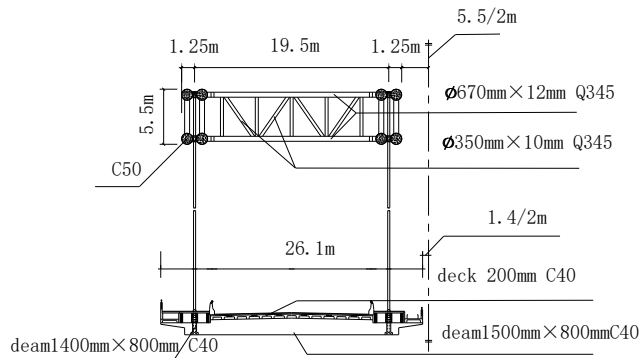


Fig. 2 Transverse cross section of the CFST arch bridge



Fig. 3 Finite element model for the bridge sample

$$\varepsilon_y \leq \varepsilon \leq \varepsilon_e \quad \sigma = f_y \quad (12)$$

where  $E_y$  is the elastic modulus of steel in this paper  $E_y=206$  GPa;  $f_y$  is yield strength of steel ( $f_y=345$  MPa);  $\varepsilon_y$  and  $\varepsilon_e$  are elastic limit strain and strengthen limit strain ( $\varepsilon_y=1.67e^{-3}$ ,  $\varepsilon_e=2.50e^{-2}$ )

$$\varepsilon \leq \varepsilon_q \quad \sigma = f_{ck} \left[ 2 \frac{\varepsilon}{\varepsilon_q} - \left( \frac{\varepsilon}{\varepsilon_q} \right)^2 \right] \quad (13)$$

$$\varepsilon_q \leq \varepsilon \leq \varepsilon_{cu} \quad \sigma = f_{ck} \left[ 1 - 0.15 \frac{\varepsilon - \varepsilon_q}{\varepsilon_{cu} - \varepsilon_q} \right] \quad (14)$$

where:  $f_{ck}$  is the peak stress of concrete, and  $f_{ck}=26.8$  MPa for C40 and  $f_{ck}=32.4$  MPa for C50;  $\varepsilon_q$  is the strain at peak stress ( $\varepsilon_q=0.002$ );  $\varepsilon_{cu}$  is the limit strain of concrete ( $\varepsilon_{cu}=0.0035$ )

$$\varepsilon \leq \varepsilon_o \quad \sigma = \sigma_o (2\varepsilon / \varepsilon_o - (\varepsilon / \varepsilon_o)^2) \quad (15)$$

$$\varepsilon \geq \varepsilon_o \quad \sigma = \begin{cases} \sigma_o \left( 1 + q \left( (\varepsilon / \varepsilon_o)^{0.1\xi} - 1 \right) \right) & (\xi \geq 1.12) \\ \sigma_o \frac{\varepsilon / \varepsilon_o}{\beta (\varepsilon / \varepsilon_o - 1)^2 + \varepsilon / \varepsilon_o} & (\xi < 1.12) \end{cases} \quad (16)$$

$$\sigma_o = \left[ 1 + (-0.054\xi^2 + 0.4\xi) (24 / f_{ck})^{0.45} \right] f_{ck}$$

$$\varepsilon_o = \varepsilon_{cc} + \left[ 1400 + 800 (f_{ck} / 24 - 1) \right] \xi^{0.2}$$

$$\varepsilon_{cc} = 1300 + 12.5 f_{ck}$$

$$q = \xi^{0.745} / (2 + \xi)$$

$$\xi = A_s f_y / A_c f_{ck}$$

$$\beta = \left( 2.36 \times 10^{-5} \right)^{0.25 + (\xi - 0.5)^7} f_{ck} \times 3.51 \times 10^{-4}$$

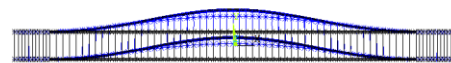
where  $\xi$  is the confinable effect coefficient.

The natural frequencies are obtained using the subspace iteration method. The natural frequencies of the first 6 modes are listed in Table 2, and the mode shapes are shown in Fig. 4.

Table 2 Dynamic characteristics of the bridge sample

Mode	1	2	3	4	5	6
Frequencies /Hz	0.28608	0.41566	0.43164	0.45876	0.54945	0.64462

ANSYS



(a) Mode 1

Fig. 4 Six typical modes

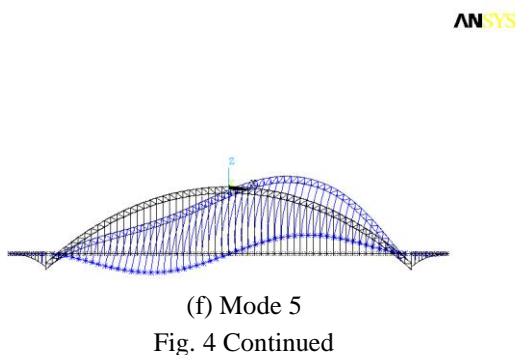
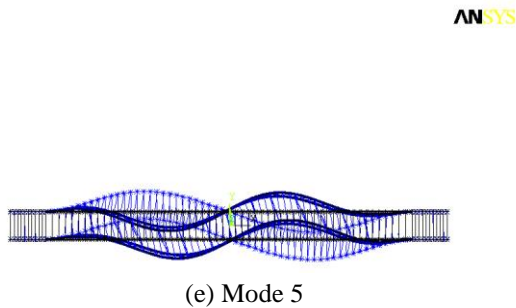
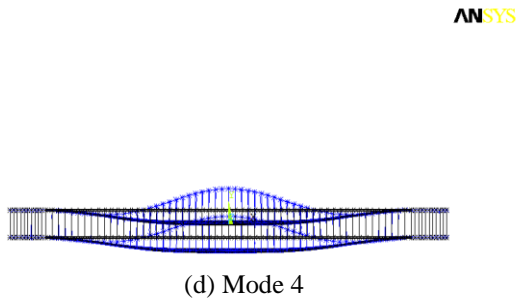
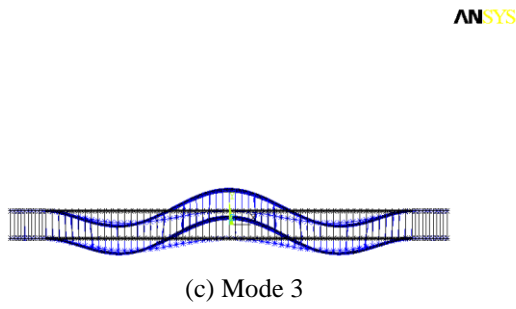
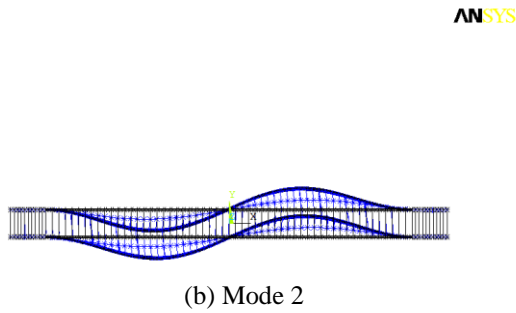


Fig. 4 Continued

**5. Selection of ground motion**

It is important to establish a relationship between ground motion intensity and structural damage. The ground motion selection is the key of the fragility analysis. In order to study the effect of wave passage, all ground motion

records should be selected from a single earthquake event. However, the lack of the near fault ground motion records makes the fragility analysis difficult. Thanks to the work of the Taiwan Strong Motion Instrumentation Program, 398 ground motion records of the 1999 Chi-Chi earthquake are available from the Pacific Earthquake Engineering Research (PEER) Center, among which only less than 40 records meet the requirement of near-fault ground motion according to the definition by Billah *et al.* (2013). To obtain more available records, the ground motion records which have source-to-site distance of less than 25 km are considered as the near-fault records. After this adjustment, more near-fault records can be obtained from the PEER and the total number of the ground motion records reaches 61.

According to the paper (Billah *et al.* 2013, Fabio and Fabio 2016), the near-fault ground motion records from recent earthquake have such characteristics: long-period velocity pulses, high ground displacements, high ratios of PGV to PGA, and high values of the ratio between the vertical and horizontal peak ground acceleration ( $\alpha_{PGA}$ ). The additional damage of structure is produced because of these characteristics of the near-fault ground motion. The selected records in this paper are divided into two parts by the ratio of PGV to PGA. The near-fault ground motion record with a high ratio is considered to have stronger near fault characteristic. In order to simulate the earthquake event, one three-dimensional ground motion record with one vertical component and two orthogonal horizontal components is selected as one ground motion sample. According to the above principle, 61 near-fault ground motion recordings are obtained from the PEER. The information of these samples is shown in Table 3.

In Table 4  $I_1$  is the damage index of bridge under uniform excitation;  $I_2$  is the damage index of bridge considering wave passage effect;  $I_3$  is the damage index of the arch rib under uniform excitation;  $I_4$  is the damage index of the arch rib considering wave passage effect;  $I_5$  is the damage index of the suspender under uniform excitation;  $I_6$  is the damage index of the suspender considering wave passage effect;  $I_7$  is the damage index of the beam under uniform excitation;  $I_8$  is the damage index of the beam considering wave passage effect.

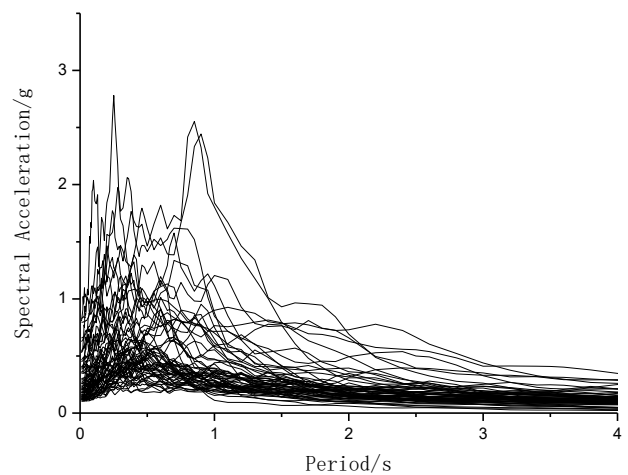


Fig. 5 Response spectra of earthquake records

Table 3a Main data of the ground motion samples

Earthquake number	$T_{H1}$ (s)	$PGA_{H1}$ (g)	$PGV_{H1}$ (m/s)	$PGV/PGA_{H1}$ (s)	$T_{H1}$ (s)	$PGA_{H2}$ (g)	$PGV_{H2}$ (m/s)	$PGV/PGA_{H2}$ (s)	$T_V$ (s)	$PGA_V$ (g)	$PGV_V$ (m/s)	$PGV/PGA_V$ (s)	$\alpha_{PGA}$	$PGV/PGA_{H,max}$
1178	3.77	0.17	0.29	0.17	4.26	0.14	0.19	0.15	4.76	0.09	0.09	0.10	0.53	0.17
1180	7.05	0.14	0.56	0.42	7.27	0.09	0.37	0.42	7.35	0.09	0.18	0.21	0.66	0.42
1182	1.67	0.36	0.42	0.12	2.57	0.30	0.60	0.20	4.10	0.22	0.20	0.09	0.60	0.20
1184	8.56	0.17	0.24	0.14	2.22	0.19	0.19	0.10	5.17	0.10	0.10	0.10	0.54	0.14
1193	6.65	0.17	0.44	0.27	5.23	0.18	0.50	0.28	5.74	0.14	0.47	0.33	0.78	0.28
1194	6.52	0.16	0.31	0.20	5.62	0.12	0.51	0.44	4.76	0.17	0.38	0.22	1.12	0.44
1197	1.07	0.69	0.55	0.08	2.61	0.58	0.61	0.11	4.33	0.34	0.26	0.08	0.49	0.11
1198	5.58	0.23	0.30	0.14	4.96	0.18	0.23	0.13	4.52	0.16	0.18	0.11	0.71	0.14
1201	1.20	0.24	0.40	0.17	1.63	0.25	0.32	0.13	7.16	0.09	0.16	0.18	0.37	0.17
1202	1.35	0.25	0.30	0.12	1.30	0.25	0.37	0.15	1.88	0.11	0.18	0.17	0.43	0.15
1203	6.96	0.20	0.41	0.21	5.07	0.27	0.36	0.14	5.95	0.11	0.14	0.14	0.39	0.21
1205	0.55	0.57	0.37	0.07	5.36	0.30	0.18	0.06	5.24	0.12	0.09	0.08	0.20	0.07
1208	3.63	0.17	0.21	0.13	2.53	0.12	0.21	0.17	7.34	0.08	0.08	0.09	0.49	0.17
1209	2.43	0.18	0.27	0.15	5.29	0.15	0.23	0.16	6.54	0.07	0.09	0.13	0.39	0.16
1227	3.77	0.16	0.21	0.13	4.71	0.23	0.29	0.13	5.36	0.10	0.15	0.15	0.43	0.13
1231	1.19	0.86	0.84	0.10	1.15	0.81	0.75	0.09	3.91	0.73	0.40	0.06	0.85	0.10
1238	6.70	0.07	0.35	0.51	5.14	0.10	0.52	0.52	6.59	0.11	0.28	0.26	1.10	0.52
1244	5.34	0.40	1.09	0.28	4.26	0.33	0.52	0.16	6.37	0.17	0.21	0.13	0.42	0.28
1246	6.20	0.18	0.53	0.30	5.75	0.15	0.56	0.39	4.21	0.13	0.33	0.26	0.73	0.39
1480	5.38	0.12	0.48	0.39	7.39	0.13	0.58	0.45	5.61	0.06	0.22	0.37	0.46	0.45
1482	5.94	0.14	0.45	0.33	9.33	0.20	0.51	0.27	5.74	0.12	0.50	0.41	0.63	0.33
1483	6.43	0.11	0.47	0.46	8.02	0.12	0.57	0.47	4.42	0.08	0.18	0.23	0.66	0.47
1486	5.14	0.10	0.25	0.24	8.04	0.12	0.29	0.25	5.90	0.10	0.22	0.23	0.81	0.25
1488	12.31	0.36	0.27	0.08	9.54	0.29	0.40	0.14	8.78	0.27	0.22	0.09	0.73	0.14
1489	6.86	0.22	0.62	0.29	10.22	0.19	0.54	0.28	7.03	0.18	0.27	0.15	0.83	0.29
1490	8.76	0.13	0.43	0.34	11.97	0.15	0.37	0.26	5.02	0.09	0.27	0.31	0.61	0.34
1491	8.81	0.24	0.42	0.18	10.38	0.16	0.39	0.25	5.83	0.11	0.29	0.27	0.46	0.25
1492	11.96	0.45	1.72	0.39	9.60	0.36	1.09	0.31	10.17	0.20	1.44	0.75	0.44	0.39
1493	9.62	0.13	0.46	0.35	13.12	0.18	0.40	0.22	6.99	0.12	0.33	0.27	0.69	0.35
1494	8.72	0.19	0.32	0.17	11.05	0.13	0.43	0.33	6.65	0.14	0.30	0.23	0.70	0.33
1495	9.32	0.17	0.35	0.20	2.93	0.23	0.26	0.11	5.98	0.14	0.39	0.28	0.60	0.20
1496	8.94	0.14	0.40	0.28	8.60	0.12	0.34	0.29	5.31	0.09	0.42	0.49	0.61	0.29
1497	8.76	0.09	0.49	0.55	13.00	0.11	0.38	0.34	5.58	0.08	0.25	0.34	0.66	0.55
1498	7.78	0.17	0.50	0.31	7.26	0.16	0.45	0.29	5.36	0.05	0.14	0.30	0.30	0.31
1499	7.51	0.10	0.37	0.37	12.43	0.11	0.33	0.32	5.31	0.09	0.26	0.30	0.82	0.37
1500	7.39	0.16	0.36	0.23	6.58	0.14	0.32	0.24	6.63	0.09	0.25	0.29	0.56	0.24
1501	6.01	0.13	0.83	0.64	6.55	0.16	0.44	0.28	4.26	0.13	0.51	0.40	0.82	0.64
1502	8.46	0.12	0.43	0.38	7.72	0.11	0.43	0.39	6.06	0.08	0.32	0.39	0.73	0.39
1503	6.74	0.36	0.92	0.26	5.74	0.79	1.25	0.16	4.86	0.26	0.69	0.27	0.33	0.26
1504	5.05	0.32	0.50	0.16	12.53	0.36	0.92	0.26	5.89	0.23	0.35	0.15	0.65	0.26
1505	12.29	0.32	2.64	0.85	13.45	0.51	1.20	0.24	10.75	0.53	2.13	0.41	1.04	0.85
1506	7.90	0.16	0.38	0.24	6.27	0.25	0.48	0.19	5.74	0.07	0.36	0.51	0.29	0.24
1507	11.12	0.57	0.68	0.12	4.10	0.50	0.52	0.11	6.45	0.42	0.38	0.09	0.75	0.12
1508	13.80	0.33	0.53	0.16	12.00	0.48	0.42	0.09	12.94	0.28	0.29	0.10	0.59	0.16
1509	1.41	0.38	0.38	0.10	1.42	0.60	0.70	0.12	3.70	0.28	0.16	0.06	0.46	0.12
1510	5.96	0.26	0.36	0.14	5.00	0.23	1.10	0.48	4.20	0.23	0.51	0.23	0.87	0.48

Table 3a Continued

Earthquake number	$T_{H1}$ (s)	$PGA_{H1}$ (g)	$PGV_{H1}$ (m/s)	$PGV/PGA_{H1}$ (s)	$T_{H1}$ (s)	$PGA_{H2}$ (g)	$PGV_{H2}$ (m/s)	$PGV/PGA_{H2}$ (s)	$T_V$ (s)	$PGA_V$ (g)	$PGV_V$ (m/s)	$PGV/PGA_V$ (s)	$\alpha_{PGA}$	$PGV/PGA_{H,max}$
1511	5.36	0.43	0.42	0.10	4.73	0.28	0.52	0.19	3.84	0.21	0.26	0.13	0.48	0.19
1512	3.92	0.25	0.23	0.09	11.97	0.42	0.30	0.07	5.65	0.17	0.17	0.10	0.42	0.09
1513	1.02	0.32	0.29	0.09	0.85	0.53	0.71	0.14	8.93	0.39	0.16	0.04	0.74	0.14
1515	8.93	0.19	0.38	0.21	8.10	0.16	0.46	0.29	6.20	0.10	0.32	0.33	0.53	0.29
1517	5.08	0.36	0.48	0.14	2.25	0.56	1.29	0.24	9.39	0.32	0.25	0.08	0.58	0.24
1519	4.99	0.11	0.31	0.27	10.40	0.11	0.30	0.29	5.36	0.09	0.49	0.54	0.82	0.29
1520	11.14	0.53	0.35	0.07	8.56	0.52	0.14	0.03	9.77	0.22	0.12	0.06	0.42	0.07
1521	7.75	0.19	0.33	0.17	5.28	0.29	0.25	0.09	5.71	0.19	0.21	0.11	0.66	0.17
1527	8.76	0.11	0.43	0.39	12.72	0.11	0.38	0.35	5.27	0.09	0.38	0.45	0.75	0.39
1528	5.72	0.26	0.30	0.12	10.32	0.21	0.41	0.20	5.19	0.17	0.47	0.29	0.65	0.20
1529	3.52	0.17	0.60	0.35	9.63	0.26	0.67	0.26	3.16	0.13	0.68	0.53	0.50	0.35
1530	7.23	0.14	0.24	0.17	8.69	0.13	0.46	0.37	6.85	0.15	0.36	0.25	1.03	0.37
1531	7.19	0.08	0.36	0.48	9.21	0.10	0.30	0.30	4.66	0.09	0.23	0.26	0.89	0.48
1532	8.32	0.12	0.36	0.30	9.53	0.11	0.33	0.30	4.59	0.06	0.18	0.31	0.49	0.30
1533	4.96	0.12	0.31	0.26	8.37	0.13	0.36	0.28	4.47	0.10	0.24	0.25	0.74	0.28

Table 3b The structural response of the ground motion samples

Earthquake Number	$DI_1$	$DI_2$	Increase percentage	$DI_3$	$DI_4$	$DI_5$	$DI_6$	$DI_7$	$DI_8$
1178	0.084	0.133	58%	0.087	0.137	0.033	0.035	0.032	0.034
1180	0.098	0.143	45%	0.102	0.148	0.033	0.035	0.030	0.034
1182	0.182	0.371	104%	0.189	0.368	0.034	0.034	0.035	0.040
1184	0.100	0.166	66%	0.104	0.171	0.032	0.032	0.035	0.037
1193	0.113	0.191	69%	0.118	0.189	0.033	0.032	0.037	0.038
1194	0.088	0.093	5%	0.095	0.097	0.034	0.035	0.029	0.028
1197	0.150	0.135	-10%	0.157	0.140	0.040	0.033	0.040	0.038
1198	0.112	0.198	77%	0.112	0.198	0.034	0.033	0.033	0.037
1201	0.187	0.203	8%	0.192	0.211	0.034	0.033	0.032	0.032
1202	0.094	0.115	22%	0.100	0.120	0.035	0.034	0.031	0.034
1203	0.128	0.196	53%	0.130	0.200	0.033	0.033	0.033	0.037
1205	0.105	0.146	40%	0.108	0.154	0.035	0.032	0.035	0.039
1208	0.099	0.120	21%	0.102	0.124	0.032	0.034	0.034	0.031
1209	0.084	0.118	41%	0.086	0.122	0.033	0.032	0.033	0.039
1227	0.082	0.063	-23%	0.089	0.067	0.034	0.034	0.028	0.024
1231	0.285	0.456	60%	0.288	0.461	0.041	0.033	0.044	0.045
1238	0.081	0.087	7%	0.086	0.094	0.034	0.037	0.034	0.031
1244	0.227	0.205	-10%	0.228	0.205	0.035	0.034	0.038	0.031
1246	0.083	0.108	31%	0.085	0.113	0.033	0.036	0.034	0.033
1480	0.089	0.117	31%	0.091	0.123	0.032	0.035	0.030	0.031
1482	0.091	0.081	-11%	0.091	0.082	0.034	0.035	0.028	0.032
1483	0.086	0.069	-19%	0.087	0.070	0.032	0.035	0.029	0.024
1486	0.075	0.080	7%	0.080	0.084	0.032	0.035	0.030	0.027
1488	0.101	0.095	-6%	0.102	0.100	0.034	0.033	0.031	0.030
1489	0.085	0.086	1%	0.090	0.086	0.035	0.033	0.033	0.026
1490	0.118	0.118	0%	0.121	0.120	0.033	0.033	0.031	0.033
1491	0.094	0.138	46%	0.096	0.137	0.035	0.033	0.027	0.036
1492	0.256	0.364	42%	0.259	0.382	0.034	0.036	0.037	0.035

Table 3b Continued

Earthquake Number	DI <sub>1</sub>	DI <sub>2</sub>	Increase percentage	DI <sub>3</sub>	DI <sub>4</sub>	DI <sub>5</sub>	DI <sub>6</sub>	DI <sub>7</sub>	DI <sub>8</sub>
1493	0.082	0.086	5%	0.089	0.089	0.034	0.033	0.031	0.031
1494	0.122	0.098	-19%	0.124	0.103	0.032	0.034	0.028	0.028
1495	0.238	0.255	7%	0.244	0.255	0.035	0.034	0.036	0.032
1496	0.108	0.114	5%	0.110	0.121	0.032	0.034	0.030	0.030
1497	0.082	0.099	20%	0.087	0.104	0.031	0.035	0.030	0.034
1498	0.104	0.126	21%	0.106	0.129	0.032	0.034	0.035	0.033
1499	0.116	0.132	14%	0.121	0.141	0.034	0.034	0.027	0.033
1500	0.101	0.120	18%	0.100	0.130	0.032	0.035	0.033	0.028
1501	0.086	0.115	34%	0.087	0.116	0.032	0.035	0.026	0.034
1502	0.101	0.109	7%	0.107	0.112	0.033	0.036	0.029	0.032
1503	0.306	0.279	-9%	0.314	0.282	0.037	0.033	0.040	0.034
1504	0.178	0.164	-8%	0.182	0.172	0.037	0.032	0.034	0.037
1505	0.176	0.238	35%	0.177	0.242	0.036	0.036	0.033	0.039
1506	0.122	0.135	10%	0.127	0.141	0.032	0.035	0.028	0.030
1507	0.417	0.356	-15%	0.429	0.366	0.039	0.032	0.042	0.036
1508	0.158	0.089	-44%	0.162	0.090	0.035	0.034	0.038	0.028
1509	0.202	0.315	56%	0.200	0.320	0.035	0.032	0.034	0.042
1510	0.095	0.102	7%	0.097	0.107	0.036	0.035	0.033	0.033
1511	0.147	0.251	71%	0.156	0.252	0.036	0.033	0.034	0.038
1512	0.213	0.200	-6%	0.219	0.209	0.035	0.033	0.035	0.035
1513	0.178	0.100	-44%	0.181	0.107	0.038	0.034	0.033	0.027
1515	0.099	0.147	49%	0.099	0.152	0.035	0.034	0.033	0.034
1517	0.181	0.433	139%	0.185	0.434	0.041	0.033	0.041	0.053
1519	0.088	0.109	25%	0.092	0.108	0.034	0.036	0.034	0.029
1520	0.215	0.275	28%	0.216	0.271	0.035	0.033	0.033	0.036
1521	0.152	0.224	48%	0.153	0.222	0.034	0.032	0.034	0.042
1527	0.094	0.111	18%	0.096	0.115	0.033	0.035	0.030	0.033
1528	0.158	0.239	51%	0.161	0.238	0.033	0.034	0.035	0.034
1529	0.086	0.092	7%	0.092	0.102	0.035	0.036	0.033	0.031
1530	0.087	0.084	-4%	0.092	0.087	0.033	0.036	0.027	0.033
1531	0.082	0.077	-5%	0.085	0.079	0.032	0.036	0.028	0.030
1532	0.107	0.131	23%	0.111	0.133	0.033	0.035	0.035	0.036
1533	0.085	0.090	6%	0.089	0.098	0.034	0.035	0.032	0.027

In Table 3 DI1 is the damage index of bridge under uniform excitation; DI2 is the damage index of bridge considering wave passage effect; DI3 is the damage index of the arch rib under uniform excitation; DI4 is the damage index of the arch rib considering wave passage effect; DI5 is the damage index of the suspender under uniform excitation; DI6 is the damage index of the suspender considering wave passage effect; DI7 is the damage index of the beam under uniform excitation; DI8 is the damage index of the beam considering wave passage effect

Table 4 The structural response of the ground motion samples

Earthquake Number	I <sub>1</sub>	I <sub>2</sub>	Increase percentage	I <sub>3</sub>	I <sub>4</sub>	I <sub>5</sub>	I <sub>6</sub>	I <sub>7</sub>	I <sub>8</sub>
1178	0.084	0.133	58%	0.087	0.137	0.033	0.035	0.032	0.034
1180	0.098	0.143	45%	0.102	0.148	0.033	0.035	0.030	0.034
1182	0.182	0.371	104%	0.189	0.368	0.034	0.034	0.035	0.040
1184	0.100	0.166	66%	0.104	0.171	0.032	0.032	0.035	0.037
1193	0.113	0.191	69%	0.118	0.189	0.033	0.032	0.037	0.038
1194	0.088	0.093	5%	0.095	0.097	0.034	0.035	0.029	0.028
1197	0.150	0.135	-10%	0.157	0.140	0.040	0.033	0.040	0.038
1198	0.112	0.198	77%	0.112	0.198	0.034	0.033	0.033	0.037
1201	0.187	0.203	8%	0.192	0.211	0.034	0.033	0.032	0.032
1202	0.094	0.115	22%	0.100	0.120	0.035	0.034	0.031	0.034
1203	0.128	0.196	53%	0.130	0.200	0.033	0.033	0.033	0.037
1205	0.105	0.146	40%	0.108	0.154	0.035	0.032	0.035	0.039
1208	0.099	0.120	21%	0.102	0.124	0.032	0.034	0.034	0.031
1209	0.084	0.118	41%	0.086	0.122	0.033	0.032	0.033	0.039
1227	0.082	0.063	-23%	0.089	0.067	0.034	0.034	0.028	0.024
1231	0.285	0.456	60%	0.288	0.461	0.041	0.033	0.044	0.045
1238	0.081	0.087	7%	0.086	0.094	0.034	0.037	0.034	0.031
1244	0.227	0.205	-10%	0.228	0.205	0.035	0.034	0.038	0.031
1246	0.083	0.108	31%	0.085	0.113	0.033	0.036	0.034	0.033
1480	0.089	0.117	31%	0.091	0.123	0.032	0.035	0.030	0.031
1482	0.091	0.081	-11%	0.091	0.082	0.034	0.035	0.028	0.032
1483	0.086	0.069	-19%	0.087	0.070	0.032	0.035	0.029	0.024
1486	0.075	0.080	7%	0.080	0.084	0.032	0.035	0.030	0.027
1488	0.101	0.095	-6%	0.102	0.100	0.034	0.033	0.031	0.030
1489	0.085	0.086	1%	0.090	0.086	0.035	0.033	0.033	0.026
1490	0.118	0.118	0%	0.121	0.120	0.033	0.033	0.031	0.033
1491	0.094	0.138	46%	0.096	0.137	0.035	0.033	0.027	0.036
1492	0.256	0.364	42%	0.259	0.382	0.034	0.036	0.037	0.035
1493	0.082	0.086	5%	0.089	0.089	0.034	0.033	0.031	0.031
1494	0.122	0.098	-19%	0.124	0.103	0.032	0.034	0.028	0.028
1495	0.238	0.255	7%	0.244	0.255	0.035	0.034	0.036	0.032
1496	0.108	0.114	5%	0.110	0.121	0.032	0.034	0.030	0.030
1497	0.082	0.099	20%	0.087	0.104	0.031	0.035	0.030	0.034
1498	0.104	0.126	21%	0.106	0.129	0.032	0.034	0.035	0.033
1499	0.116	0.132	14%	0.121	0.141	0.034	0.034	0.027	0.033
1500	0.101	0.120	18%	0.100	0.130	0.032	0.035	0.033	0.028
1501	0.086	0.115	34%	0.087	0.116	0.032	0.035	0.026	0.034
1502	0.101	0.109	7%	0.107	0.112	0.033	0.036	0.029	0.032
1503	0.306	0.279	-9%	0.314	0.282	0.037	0.033	0.040	0.034
1504	0.178	0.164	-8%	0.182	0.172	0.037	0.032	0.034	0.037
1505	0.176	0.238	35%	0.177	0.242	0.036	0.036	0.033	0.039
1506	0.122	0.135	10%	0.127	0.141	0.032	0.035	0.028	0.030
1507	0.417	0.356	-15%	0.429	0.366	0.039	0.032	0.042	0.036
1508	0.158	0.089	-44%	0.162	0.090	0.035	0.034	0.038	0.028
1509	0.202	0.315	56%	0.200	0.320	0.035	0.032	0.034	0.042
1510	0.095	0.102	7%	0.097	0.107	0.036	0.035	0.033	0.033

Table 4 Continued

Earthquake Number	I <sub>1</sub>	I <sub>2</sub>	Increase percentage	I <sub>3</sub>	I <sub>4</sub>	I <sub>5</sub>	I <sub>6</sub>	I <sub>7</sub>	I <sub>8</sub>
1511	0.147	0.251	71%	0.156	0.252	0.036	0.033	0.034	0.038
1512	0.213	0.200	-6%	0.219	0.209	0.035	0.033	0.035	0.035
1513	0.178	0.100	-44%	0.181	0.107	0.038	0.034	0.033	0.027
1515	0.099	0.147	49%	0.099	0.152	0.035	0.034	0.033	0.034
1517	0.181	0.433	139%	0.185	0.434	0.041	0.033	0.041	0.053
1519	0.088	0.109	25%	0.092	0.108	0.034	0.036	0.034	0.029
1520	0.215	0.275	28%	0.216	0.271	0.035	0.033	0.033	0.036
1521	0.152	0.224	48%	0.153	0.222	0.034	0.032	0.034	0.042
1527	0.094	0.111	18%	0.096	0.115	0.033	0.035	0.030	0.033
1528	0.158	0.239	51%	0.161	0.238	0.033	0.034	0.035	0.034
1529	0.086	0.092	7%	0.092	0.102	0.035	0.036	0.033	0.031
1530	0.087	0.084	-4%	0.092	0.087	0.033	0.036	0.027	0.033
1531	0.082	0.077	-5%	0.085	0.079	0.032	0.036	0.028	0.030
1532	0.107	0.131	23%	0.111	0.133	0.033	0.035	0.035	0.036
1533	0.085	0.090	6%	0.089	0.098	0.034	0.035	0.032	0.027

It is noticed from the Table 4 that I<sub>1</sub> and I<sub>2</sub> are significantly affected by I<sub>3</sub> and I<sub>4</sub>. The reason for this phenomenon is that the amount of the cumulative hysteretic energy in the arch rib is much more than that in the other parts. The damage of the arch rib is significantly affected by the wave passage effect but this effect in the suspender and the beam are not so obvious. The damage index in the arch rib is higher than that in other parts of the bridge. This means the seismic damage is concentrated at the arch rib, which indicates the arch rib is the main supporting structure in the bridge.

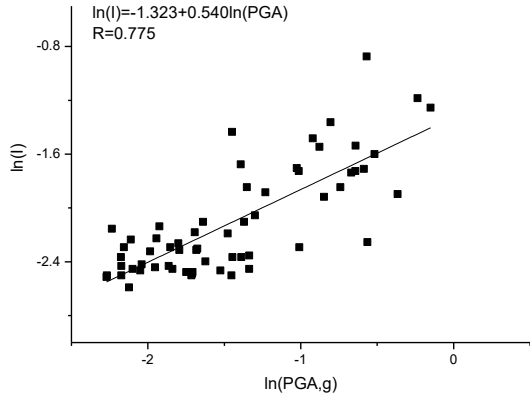
## 6. Uniform excitation

The wave passage effect is not involved in this analysis. Each sample is calculated by the FEA program to obtain the seismic response. According to the damage model mentioned above, the damage indexes are calculated using these seismic responses. The relationship between the seismic response and the ground motion intensity is linear in log-log coordinate (Karim *et al.* 2009). The relationship between the damage index and the ground motion intensity is shown in Fig. 6.

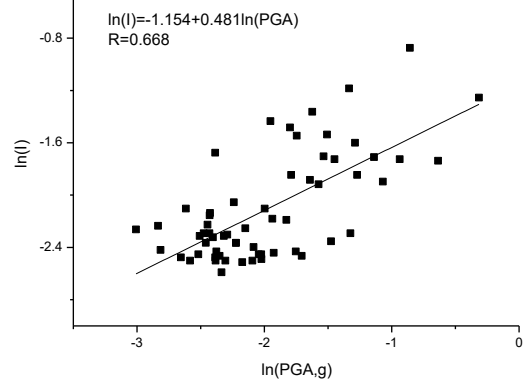
The probability of the bridge in a certain damage state is shown

$$P_f = P[I > I_i] = \Phi \left[ \frac{\ln \left( \frac{I}{I_i} \right)}{\beta} \right] \quad (17)$$

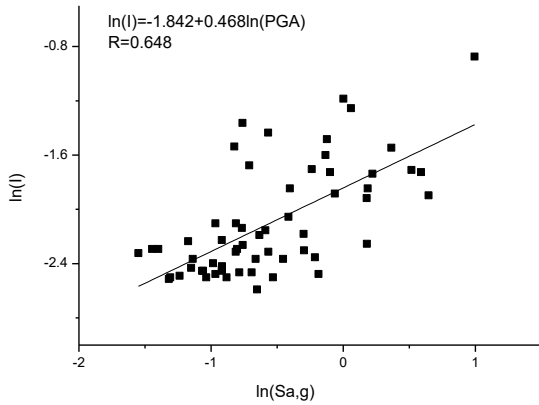
For example, the probability of the slight damage state is defined as follows



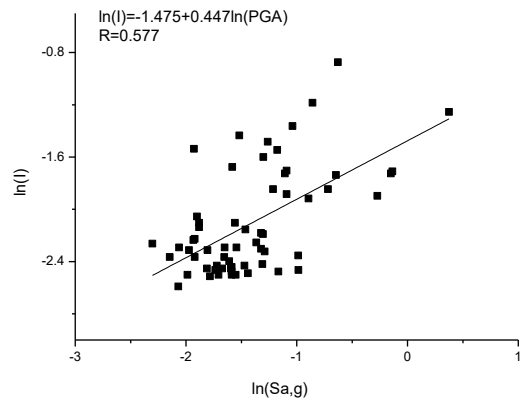
(a) Regression relation of damage index with the horizontal PGA



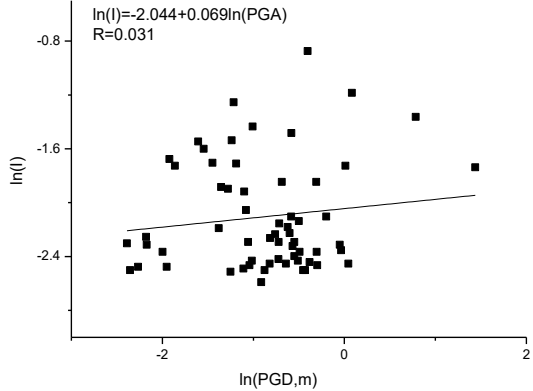
(b) Regression relation of damage index with the vertical PGA



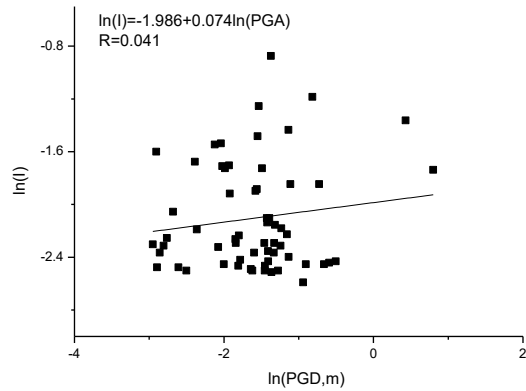
(c) Regression relation of damage index with the horizontal Sa



(d) Regression relation of damage index with the vertical Sa



(e) Regression relation of damage index with the horizontal PGD



(f) Regression relation of damage index with the vertical PGD

Fig. 6

$$P_f = P[I > I_1 | \text{PGA}] = \Phi \left[ \frac{\ln\left(\frac{I}{0.10}\right)}{0.775} \right] \quad (18)$$

$$\ln(I) = -1.290 + 0.557 \ln(\text{PGA}) \quad (19)$$

The fragility curves of the bridge sample are shown in Fig. 7.

Fig. 6 shows that the slopes of the regression curves of damage index with PGD are lower than 0.1, while the slopes of the PGA and Sa curves are higher than 0.4. This

shows that the influence of the PGA and  $S_a$  on the damage index is more obvious than that of the PGD. Based on this bridge model, the PGA and the  $S_a$  are appropriate measures of ground motion intensity. Then fragility curves of the PGA and  $S_a$  are obtained. From Fig. 7, the horizontal PGA medians of the slight damage and moderate damage are respectively 0.17 g and 1.27 g, and the horizontal PGA medians are respectively 0.10g and 0.95 g. The horizontal and the vertical  $S_a$  medians of the slight damage are 0.40 g and 0.16 g, respectively. A conclusion can be drawn that the vertical ground motion component is more destructive than the horizontal component. The medians of the extensive

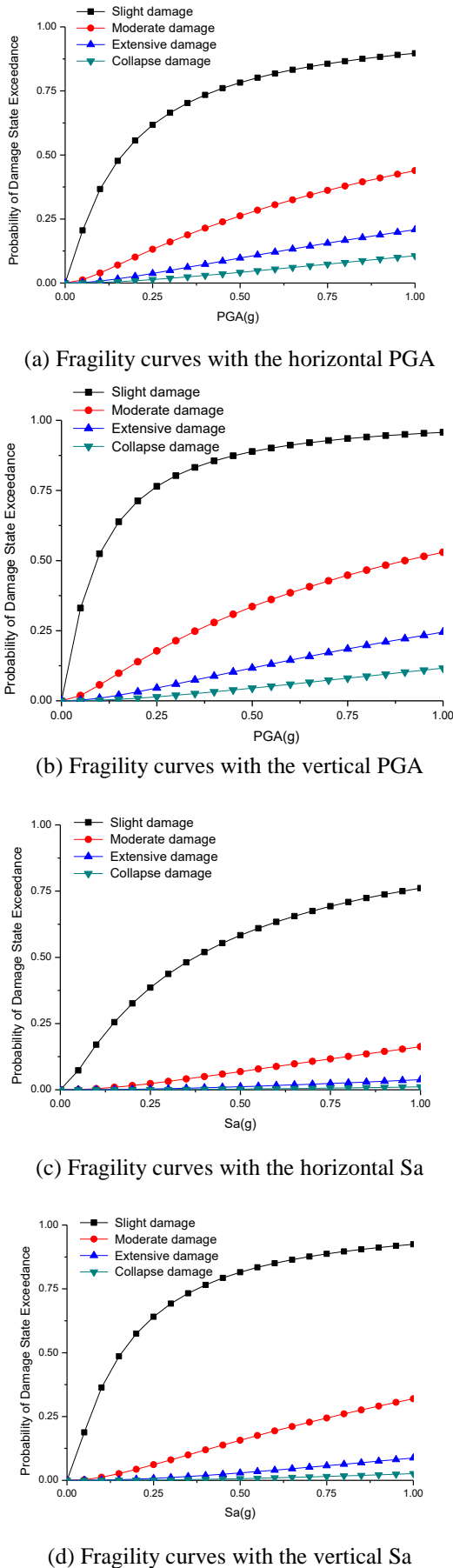


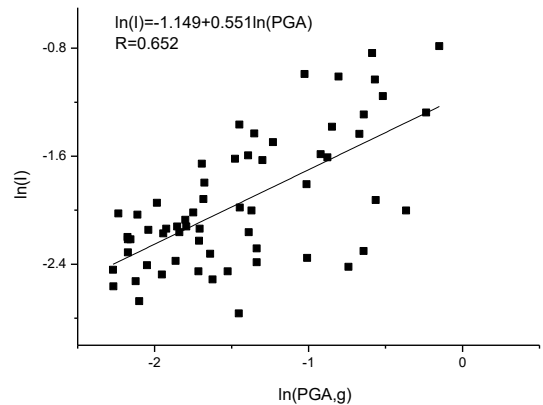
Fig. 7

damage and collapse damage are beyond the PGA and Sa range of ground motion samples.

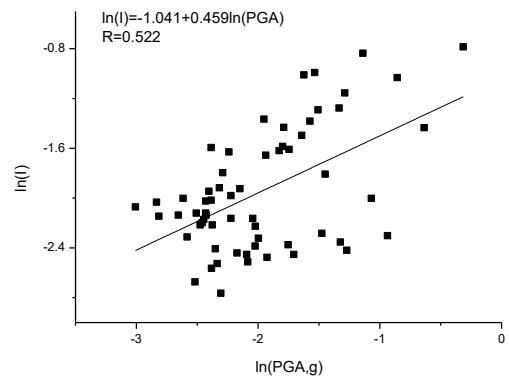
### 7. Non-uniform excitation

The ground motion sample is inputted at eight locations of the bridge model. Because the time of earthquake waves propagating along direction of length side is much longer than width short side, the two transverse input locations are merged into one. After this merging, the ground motion is inputted at four locations (the two abutments, the two arch springers). Due to the symmetry of the structure, the left abutment is assumed to be close to the source of the earthquake so the other three locations exits a short time lag. The angle between the bridge longitudinal direction and the seismic wave propagation direction is randomly produced, as well as the seismic wave velocity. The seismic wave velocity ranges from 200 m/s to 1000 m/s (Mehanny *et al.* 2014). The time lag is calculated by projection length of the bridge in the seismic wave propagation direction and the seismic wave velocity.

When the wave passage effect is considered, the average of the damage index is increased by 21%, the largest increment is 139% and the largest reduction is 44%. The number of the samples whose damage indexes are increased

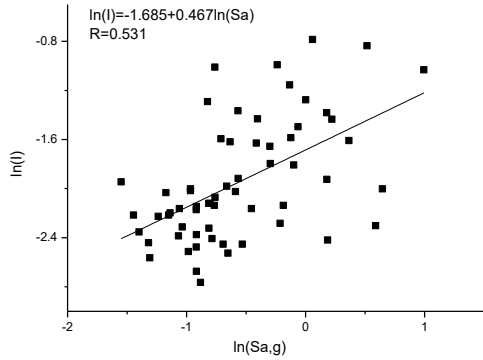


(a) Regression relation of damage index with the horizontal PGA considering the wave passage effect

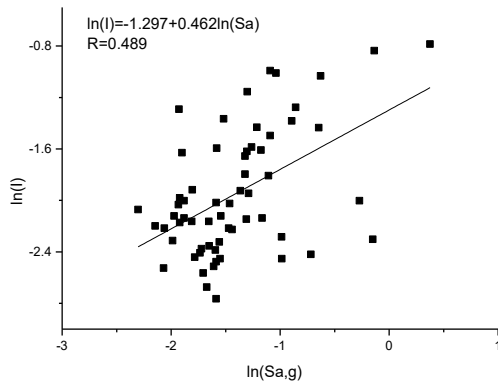


(b) Regression relation of damage index with the vertical PGA considering the wave passage effect

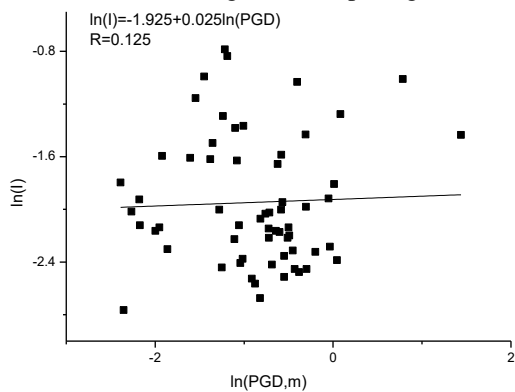
Fig. 8



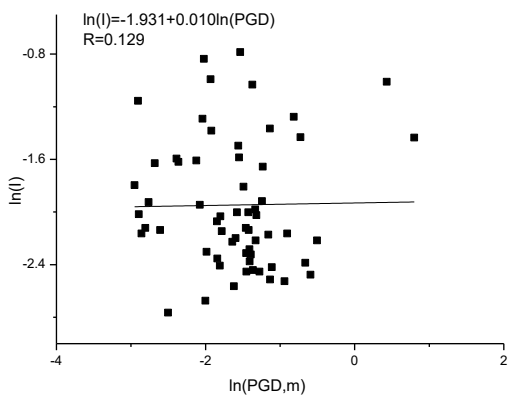
(c) Regression relation of damage index with the horizontal Sa considering the wave passage effect



(d) Regression relation of damage index with the vertical Sa considering the wave passage effect

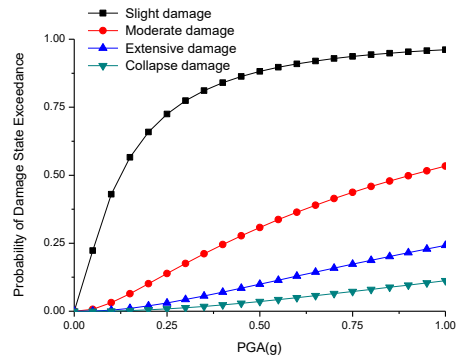


(e) Regression relation of damage index with the horizontal PGD considering the wave passage effect

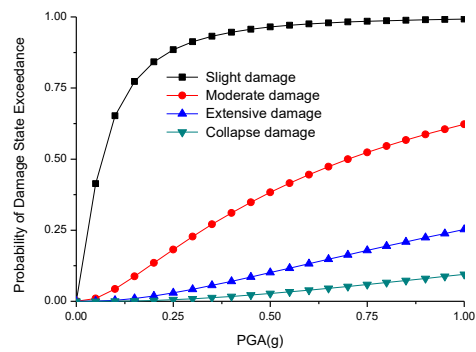


(f) Regression relation of damage index with the vertical PGD considering the wave passage effect

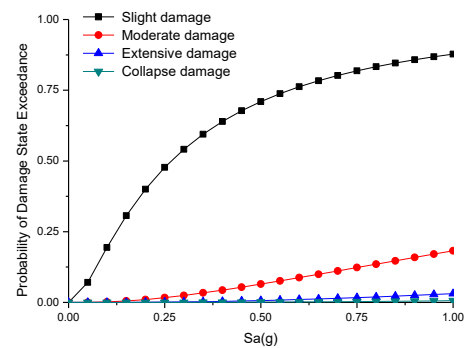
Fig. 8 Continued



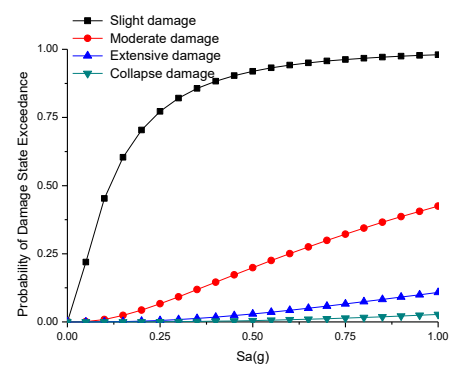
(a) Fragility curves with horizontal PGA considering the wave passage effect



(b) Fragility curves with the vertical PGA considering the wave passage effect



(c) Fragility curves with horizontal Sa considering the wave passage effect



(d) Fragility curves with the vertical Sa considering the wave passage effect

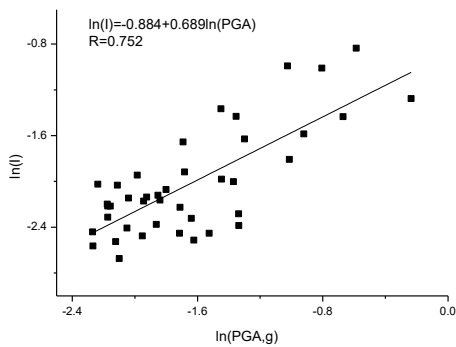
Fig. 9

is 45, which take up 73.77% of the total number. According to the ground motion samples used in this work, the changes of the damage indexes are not directly or obviously related to the time lag. This may be explained by the complexity of the ground motion records used in this work.

The relationship between the damage index and the ground motion intensity is obtained by the method which is used to analyze the uniform excitation case. The relationship is shown as Fig. 8. Then the fragility curves of the bridge are obtained and these fragility curves are drawn in Fig. 9. Comparing with the result of the uniform excitation case, when the wave passage effect is considered, the dispersion of the damage index is increased and the ground motion intensity increment causes more the damage index increment.

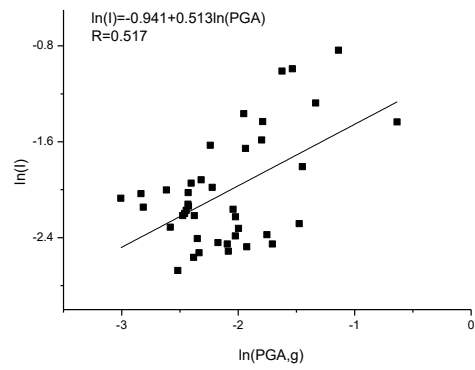
Comparing with the uniform excitation case, when the wave passage effect is considered, the failure probability of each damage state is increased. The medians of the slight damage and moderate damage are reduced. The medians of horizontal PGA are changed from 0.17 g and 1.27 g to 0.13 g and 0.90 g, respectively. The medians of vertical PGA are changed from 0.10 g and 0.95 g to 0.07 g and 0.70 g, respectively. Similar phenomenon can be observed from the Fig. 9(d) and Fig. 9(e). The median of horizontal Sa is changed from 0.40 g to 0.27 g. The medians of vertical Sa is changed from 0.16 g to 0.11 g. The medians of moderate damage are beyond the Sa range of ground motion samples. For this bridge model, PGD is not an appropriate ground motion intensity measure so this measure is not involved in further study. A conclusion can be drawn that damages can be enlarged by considering the wave passage effect.

The ground motion samples are divided into two parts by the ratio of PGV to PGA. If the ratio is greater than 0.2, the ground motion sample is considered possessing the strong characteristic of near-fault. If the ratio is less than 0.2, the characteristic of near-fault is not so strong. The additional damage which caused by wave passage effect may be changed by the ratio. The two sets of data which is divided by the ratio are analyzed separately. The fragility curves are developed to study the change of the damage index. By using the above method, the relationship and the fragility curves are obtained as Figs. 10 to 13.

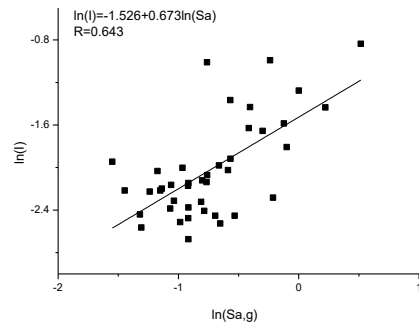


(a) Regression relation of damage index with the horizontal PGA considering the wave passage effect based on the high ratio group data

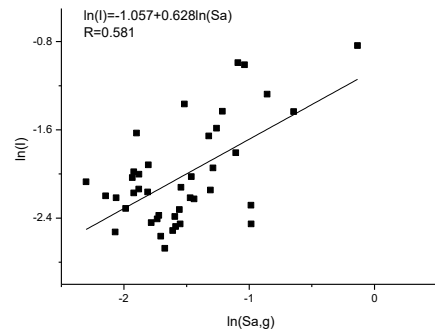
Fig. 10



(b) Regression relation of damage index with the vertical PGA considering the wave passage effect based on the high ratio group data

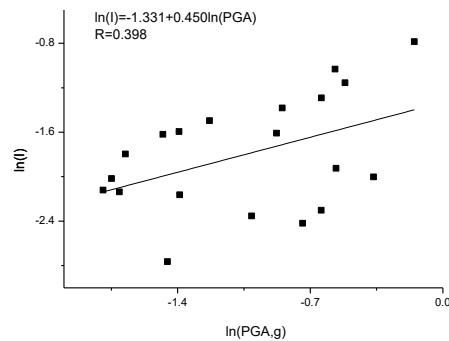


(c) Regression relation of damage index with the horizontal Sa considering the wave passage effect based on the high ratio group data



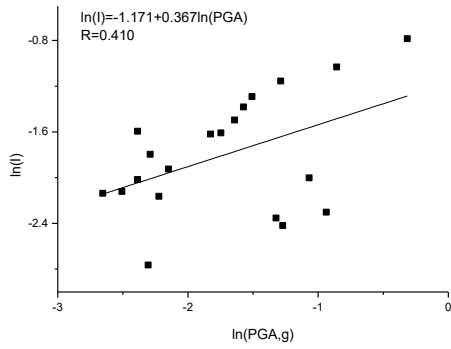
(d) Regression relation of damage index with the vertical Sa considering the wave passage effect based on the high ratio group data

Fig. 10 Continued

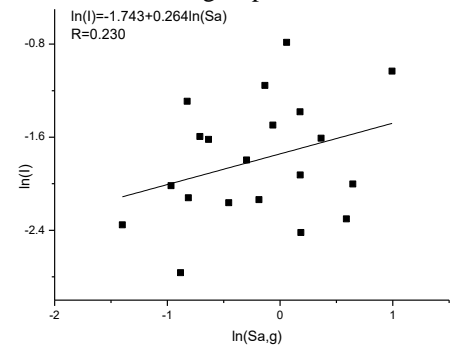


(a) Regression relation of damage index with the horizontal PGA considering the wave passage effect based on the low ratio group data

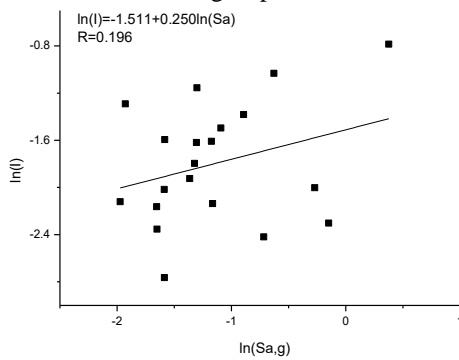
Fig. 11



(b) Regression relation of damage index with the vertical PGA considering the wave passage effect based on the low ratio group data

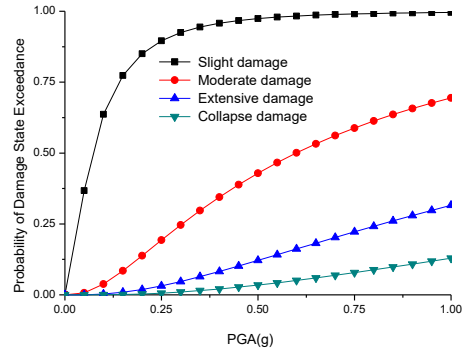


(c) Regression relation of damage index with the horizontal Sa considering the wave passage effect based on the low ratio group data

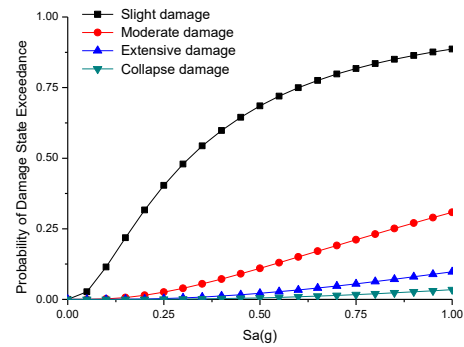


(d) Regression relation of damage index with the vertical Sa considering the wave passage effect based on the low ratio group data

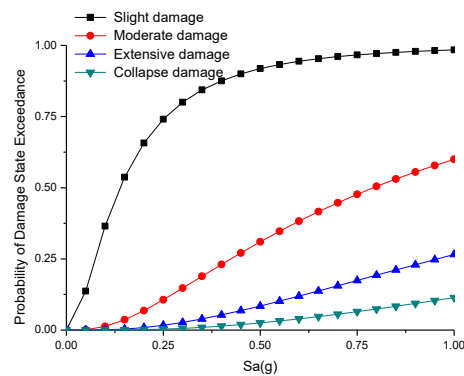
Fig. 11 Continued



(b) Fragility curves with the vertical PGA considering the wave passage effect based on the high ratio group data

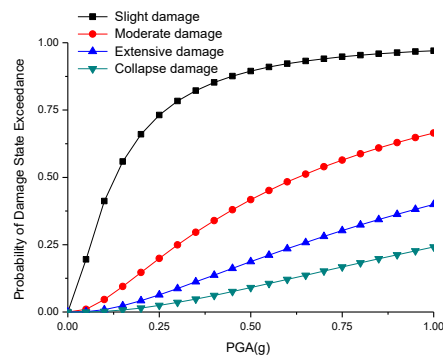


(c) Fragility curves with the horizontal Sa considering the wave passage effect based on the high ratio group data



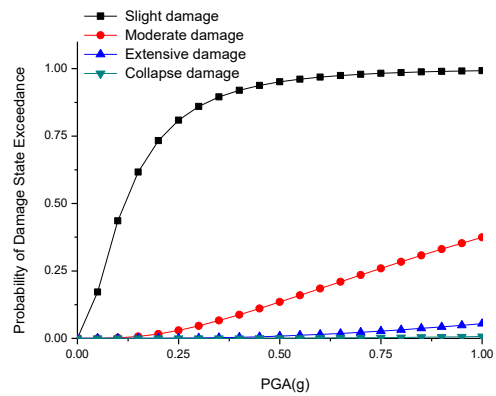
(d) Fragility curves with the vertical Sa considering the wave passage effect based on the high ratio group data

Fig. 12 Continued



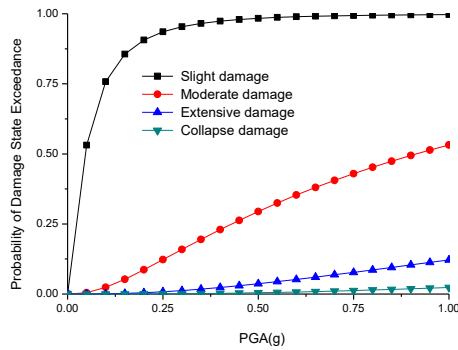
(a) Fragility curves with the horizontal PGA considering the wave passage effect based on the high ratio group data

Fig. 12

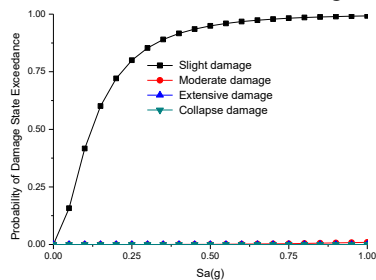


(a) Fragility curves with the horizontal PGA considering the wave passage effect based on the low ratio group data

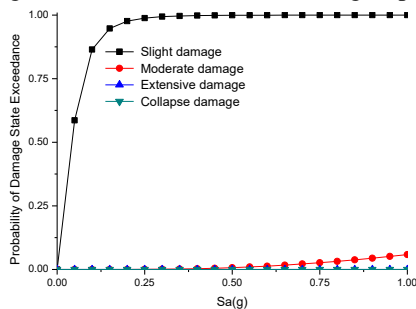
Fig. 13



(b) Fragility curves with the vertical PGA considering the wave passage effect based on the low ratio group data



(c) Fragility curves with the horizontal Sa considering the wave passage effect based on the low ratio group data



(d) Fragility curves with the vertical Sa considering the wave passage effect based on the low ratio group data

Fig. 13 Continued

Fig. 10 and Fig. 11 show that the slope of the high ratio group is larger than those of the low ratio group. This means that more damage can be caused by the same ground motion intensity increment in the high ratio group. The effect is more obvious in the fragility curves of the vertical ground motion component than those of the horizontal ground motion component. When Sa is used as ground motion intensity, the phenomenon is more obvious. It can be observed from the Figs. 12 and 13 that the failure probability of the high ratio group is higher than that of the low ratio group in moderate damage state, extensive damage state and collapse damage state. When PGA is used as ground motion intensity, the increase of the failure probability is 10%-20%. When Sa is used as ground motion intensity, the increase of the failure probability reaches 50% and the failure probability of the low ratio group of moderate damage or above is less than 5%. This means that moderate damage state cannot be caused by these ground motions of the low ratio group. This increase in slight damage state is not obvious and in some ground motion

intensity the slight damage failure probability of the high ratio group is less than that of the low ratio group. The intercept of regression relation may explain this phenomenon. Comparing with the uniform excitation case, the ground motion record with a high ratio of PGV to PGA is more likely to cause greater additional damage due to the wave passage effect in the same condition. It can be concluded that the damage of the wave passage effect can be increased by the near-fault ground motion records.

## 8. Conclusions

This paper presents the seismic fragility analyses of a typical CFST arch bridge to evaluate the wave passage effect. In order to study the wave passage effect, the ground motion records used in this paper are selected in a single earthquake event. The near-fault ground motion record is proved to make the wave passage effect more obvious. According to the seismic fragility analyses, the main conclusions can be summarized as follows:

1. For this bridge model, Sa and PGA are appropriate measures of ground motion intensity. The influences of Sa and PGA on the damage index are more serious than that of the PGD. The vertical ground motion component is more destructive than the horizontal ground motion component under the same ground motion intensity whether the wave passage effect is considered or not.

2. When the wave passage effect is considered, the average of the damage indexes is increased by 21%. The number of the samples whose damage indexes are increased is 45, which takes up 73.77% of the total number. The seismic damage is increased by considering the wave passage effect. Under the non-uniform excitation, the failure probability of each damage state is increased. The medians of the PGA are reduced by 20%-30% basing on the slight damage state and the moderate state. This reduction of Sa is more than 30%. The damage of the bridge will be underestimated if the wave passage effect is ignored.

3. The wave passage effect can be intensified by the near-fault ground motion records. A record with a high ratio PGV to PGA is more likely to increase the additional damage caused by the wave passage effect. When Sa is used as ground motion intensity, the increase of additional damage is more obvious and the increase of the failure probability of the moderate damage can reach 50%. For extensive damage and collapse damage, the increase of the failure probability is 10%. The failure probability of the low ratio group of moderate damage is less than 5%.

## Acknowledgements

This work was supported by National Natural Science Foundation of China under Grant no. 51178080. The author would like to thank the Pacific Earthquake Engineering Research (PEER) Center for the earthquake data. Finally, the author would like to thank the comments and suggestions of two anonymous reviewers.

## References

- Billah, A.H.M.M., Alam, M.S. and Bhuiyan, M.A.R. (2012), "Fragility analysis of retrofitted multicolumn bridge bent subjected to near-fault and far-field ground motion", *J. Bridge Eng.*, **18**(10), 992-1004.
- Deodatis, G., Saxena, V. and Shinozuka, M. (2000), "Effect of spatial variability of ground motion on bridge fragility curves", *Proceeding of 8th Specialty Conference on Probabilistic Mechanics and Structural Reliability*.
- Hsu, Y.T. and Fu, C.C. (2004), "Seismic effect on highway bridges in Chi Chi earthquake", *J. Perform. Constr. Fac.*, **18**(1), 47-53.
- Hwang, H., Liu, J.B. and Chiu, Y.H. (2001), "Seismic fragility analysis of highway bridges", Mid-America Earthquake Center CD Release 01-06.
- Karim, K.R. and Yamazaki, F. (2000), "Comparison of empirical and analytical fragility curves for RC bridge piers in Japan", *8th ASCE Specialty Conference on Probabilistic Mechanics and Structural Reliability*, ASCE, CD-ROM.
- Karim, K.R. and Yamazaki, F. (2007), "Effect of isolation on fragility curves of highway bridges based on simplified approach", *Soil Dyn. Earthq. Eng.*, **27**(5), 414-426.
- Kim, S.H. and Feng, M.Q. (2003), "Fragility analysis of bridges under ground motion with spatial variation", *Int. J. Non-Linear Mech.*, **38**(5), 705-721.
- Mazza, F. and Alesina, F. (2016), "Effects of site condition in near-fault area on the nonlinear response of fire-damaged base-isolated structures", *Eng. Struct.*, **111**, 297-311.
- Mehanny, S.S.F., Ramadan, O.M.O. and El Howary, H.A. (2014), "Assessment of bridge vulnerability due to seismic excitations considering wave passage effects", *Eng. Struct.*, **70**, 197-207.
- Park, Y.J. and Ang, A.H.S. (1985), "Mechanistic seismic damage model for reinforced concrete", *J. Struct. Eng.*, **111**(4), 722-739.
- Park, Y.J., Ang, A.H.S. and Wen, Y.K. (1985), "Seismic damage analysis of reinforced concrete buildings", *J. Struct. Eng.*, **111**(4), 740-757.
- Rodriguez, M.E. and Padilla, D. (2009), "A damage index for the seismic analysis of reinforced concrete members", *J. Earthq. Eng.*, **13**(3), 364-383.
- Saxena, V. (2000), "Spatial variation of earthquake ground motion and development of bridge fragility curves", Degree of Doctor of Philosophy, Department of Civil Engineering and Operations Research, Princeton University.
- Shin, T.C., Kuo, K.W., Lee, W.H.K., Teng, T.L. and Tsai, Y.B. (2000), "A preliminary report on the 1999 Chi-Chi (Taiwan) earthquake", *Seismol. Res. Lett.*, **71**(1), 24-30.
- Somerville, P.G. (2002), "Characterizing near fault ground motion for the design and evaluation of bridges", *Third National Conference and Workshop on Bridges and Highways*, Portland, Oregon, April.
- Somerville, P.G., Smith, N.F., Graves, R.W. and Abrahamson, N.A. (1997), "Modification of empirical strong ground motion attenuation relations to include the amplitude and duration effects of rupture directivity", *Seismol. Res. Lett.*, **68**(1), 199-222.
- Todorovska, M.I. and Trifunac, M.D. (1989), "Antiplane earthquake waves in long structures", *J. Eng. Mech.*, **115**(12), 2687-2708.
- Wang, J., Zhang, M.Z. and Guo, X.L. (2009), "Nonlinear stability analysis on the concrete casting step of long-span concrete-filled steel tube arch bridge", *Materials Science Forum*, Trans Tech Publications, **614**, 275-282.
- Xie, K.Z., Lu, W.G., Qin, L.Q. and Meng, F.C. (2012), "Research on seismic damage evaluation of CFST arch bridges", *Zhongguo Gonglu Xuebao(China Journal of Highway and Transport)*, **25**(2), 53-59.
- Zhang, Y.H., Li, Q.S., Lin, J.H. and Williams, F.W. (2009), "Random vibration analysis of long-span structures subjected to spatially varying ground motions", *Soil Dyn. Earthq. Eng.*, **29**(4), 620-629.

CY